important that young students and researchers throughout the world recognize rapid development of the Project and that they endeavour to solve the lamental issues that must be overcome in ITER.

REFERENCES

da, *J. Plasma Fusion Res.* **84**, 3 (2008).

The Physics Basis of ITER Confinement

F. Wagner

Max-Planck-Institut für Plasmaphysik
EURATOM Association
Wendelsteinstr. 1, 17491 Greifswald, Germany

Abstract. ITER will be the first fusion reactor and the 50 year old dream of fusion scientists will become reality. The quality of magnetic confinement will decide about the success of ITER, directly in the form of the confinement time and indirectly because it decides about the plasma parameters and the fluxes, which cross the separatrix and have to be handled externally by technical means. This lecture portrays some of the basic principles which govern plasma confinement, uses dimensionless scaling to set the limits for the predictions for ITER, an approach which also shows the limitations of the predictions, and describes briefly the major characteristics and physics behind the H-mode – the preferred confinement regime of ITER.

Keywords: confinement, tokamaks, ITER, H-mode
PACS: 52.55.Fa

1. INTRODUCTION

ITER will be the first fusion reactor – a device which will deliver energy based on fusion reactions at a rate by far larger than the power invested to produce and maintain the burning plasma state. The goal for ITER is the production of 500 MW of total fusion power for 400 seconds; the power amplification factor $Q = P_{fus}/P_{aux}$ is projected to be about 10.

ITER is based on the tokamak concept as it has been developed over the last 50 years. International fusion research started with the Geneva IAEA conference in 1958. The T3 tokamak of the Kurchatov Institute in Moscow demonstrated the basic confinement capability of the tokamak and made this concept to the front runner in magnetic confinement R&D. Many research institutions have been contributing to the tokamak development and the ITER design rests on the results of about 40 devices operated or still operating world-wide [1]. Recently, new tokamaks started operation – SST-1 in India, EAST in China and KSTAR in Korea. Many tokamaks contributed to the physics and understanding of high-temperature plasma phenomena – equilibrium, stability, confinement, exhaust and plasma-wall interaction, heating, current-drive, diagnostics, as well as performance optimisation and fusion technology. Specific design contributions to ITER came from ASDEX, which developed a relevant divertor concept in the 80ies and discovered the H-mode – the confinement regime foreseen for ITER - and JET the presently largest fusion device with parameters closest to those predicted for ITER. JET pioneered high-current plasmas with elliptical cross-section and has produced plasmas with Q = 0.65 [2].

CP1095, *2nd ITER International Summer School: Confinement*
edited by: S.-I. Itoh, S. Inagaki, M. Shindo, and M. Yagi

:R is the acronym for International Thermonuclear Experimental Reactor. The indicates that ITER will not be exclusively a targeted demonstration device but is rather the next step in the development of fusion energy, however with well d scientific and technological goals. The major open issues to be addressed by are:

- to produce fusion power and provide α-particle heating at a level which surpasses the external heating power;
- to develop the means to control the fusion burn;
- to study instabilities as they may be driven specifically by the slowing-down spectrum of the α-particles;
- to develop long-pulse scenarios and techniques to qualify the tokamak for steady-state operation;
- to test a blanket module and confirm the necessary tritium breeding ratio of ~ 1.1.

:h ITER, a tremendous research and development programme culminates and will finally delivers what has been promised in the middle of last century.

2. THE DESIGN OF ITER

ng a tokamak, the ITER plasma is confined in toroidal geometry [3]. The al field (5.3 T on axis, see Fig. 1) and the poloidal field from a strong toroidal ıt I_p (15 MA) provide the helical field structure with rotational transform ι. ITER ı aspect ratio of $A = R_0/a = 3.1$ which is an empirically well confirmed design

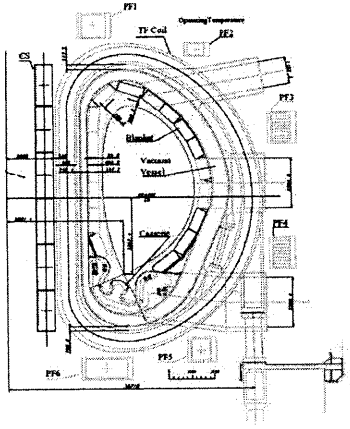

Major radius	6.2 m
Minor radius	2.0 m
Toroidal field	5.3 T
Plasma current	15 MA
Elongation κ	1.85
Triangularity δ	0.49
Fusion power	400-500 MW
Q	~10
Burn duration	~ 400 s

GURE 1. Cross-section of the ITER device with the elliptical and triangular shape of the plasma; table of major design parameters and objectives of ITER [4].

e ITER performance is expected to strongly benefit in confinement and tional range from strong shaping of the plasma cross-section. The optimization

of the flux surface geometry is restricted, however, to axi-symmetric shaping. The ITER poloidal cross-section is shown in Fig. 1 along with a table of major parameters. The elongation of $\kappa = 1.85$ allows ITER to obey the q-limit and operate safely at high current. The safety factor $q\ (=2\pi/\iota) \sim 5\ a^2\ (B/RI_p)\ ((1+\kappa^2)/2)$ (T, MA, m).

The q_{95}-value (at the 95% flux surface - a measure of the global q-value) of ITER is 3.0 and is again a typical value for optimal and safe plasma operation. With elongation, higher I_p values can be operated (at specified q) which allow to expand the operational range in density and beta (= ratio of average kinetic to magnetic pressure ~ $<p>/B^2$). The density is limited in tokamaks by the Greenwald limit ($n_e \leq I_p/a^2$) [5] and beta by the Troyon limit ($\beta \leq \beta_N I_p/aB$) [6] – all scale with current. Also the tokamak confinement time τ_E scales with plasma current (see equ. 1).

Another important geometrical parameter in the design of tokamaks is triangularity. This feature improves stability and specifically confinement when approaching the density limit. Figure 2 shows the decrease of the confinement time τ_E (in normalized form) with density (normalized against the Greenwald density) for various values of triangularity. ITER will operate at $n_e/n_{GW} = 0.85$. The data shown in Fig. 2 are obtained by JET [7] and confirmed by others. Triangularity does not avoid the density induced confinement degradation but allows to restores the targeted level.

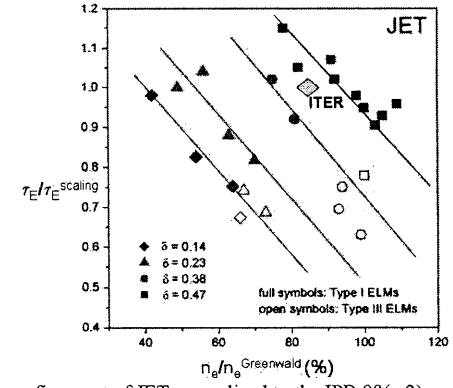

FIGURE 2. The confinement of JET normalized to the IPB 98(y,2) scaling versus density, normalized against the Greenwald limit for JET with the triangularity as parameter [7]. The ITER target point is also shown.
Reprinted with permission of IOP Publishing.

The size of ITER is also determined by technical considerations – e.g. by the space for the central ohmic transformer and the inner legs of the coils. The size of the plasma - the minor radius a (at specified A) – must provide the necessary thermal insulation to provide the core temperatures of about 20 keV with a confinement time τ_E, which fulfills the Lawson ignition and burn conditions. The confinement time is determined by the radial fluxes from the plasma core across the edge, which are largely based on turbulent processes. The crucial triple product $nT\tau_E$ of $6\ 10^{21}\ m^{-3}$ keV s for ITER necessitates a minor radius of 2 m providing the necessary thermal insulation under H-mode operational conditions (see chapt. 8).

ure 3 shows the experimental τ_E values of 9 tokamaks of different sizes and
; but which all operate in the ELMy H-mode (see chapt. 8) [8]. They establish
ta base which allows extrapolation to ITER. The expected energy confinement
or ITER in 50-50% DT operation is 3.7 s.

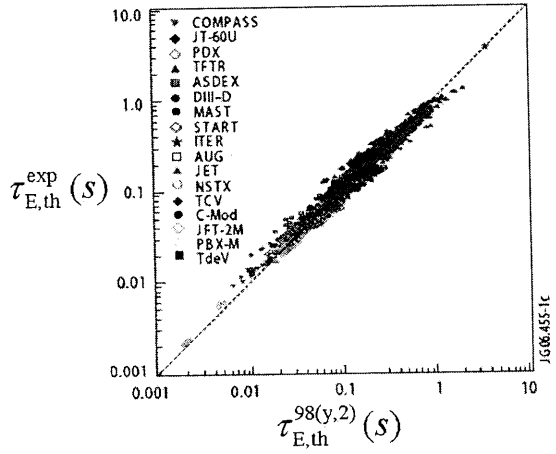

FIGURE 3. Multi-machine scaling in the ELMy H-mode. Experimental data points are plotted
st the regression analysis which let to the IPB 98(y,2) ITER scaling [8]. The ITER target point is
also plotted.
Reprinted with permission of IOP Publishing.

is an aggravating element for fusion development that - unlike fission - the basic
iple and many physics issues and technologies and their interplay can only be
nstrated in an experimental device of reactor size and at the reactor power level.
oper confinement is only one of the requirements for successful operation. The
. plasma has to be started and terminated with an economic handling of the
able inductive flux. It has to be properly heated and non-inductive current drive
o be developed – issues partly of particle-wave interaction; the helium ash has to
moved from the plasma core (after the α-particles have slowed down), which is
esult of a complex interplay between diffusive transport for He, a possible inward
in transport, the retention capability of the divertor and the overall control of
cling. The impurity concentration has to be low to avoid excessive Z_{eff} (<1.8)
es and resulting core impurity radiation levels. These requirements affect
tions of wall materials, erosion mechanisms, impurity transport characteristics and
occurrence of ELMs (edge localised modes; see chapt. 8.5) to prevent the
ection of impurities to the core or sawteeth to purge the plasma core.
able operation demands to obey the operational limits for q, β, elongation and
ity. Technical means have to be prepared to suppress neo-classical tearing modes
injection of electron cyclotron waves). The external heating power has to surpass
power threshold P_{LH} for the H-mode [9]. A good data base is available for
erium plasmas; the necessary power for the H-mode in ITER is about 50 MW.

The empirically observed dependence of P_{LH} on the isotopic mass is also of interest. Hydrogen or He as working gas is foreseen during the initial non-nuclear operational period for system testing and optimisation. The H-mode power threshold in hydrogen is, however, a factor of 2 larger to that of deuterium [10].

A detailed account of the ITER physics basis is given in Ref. [4]; chapt. 2 "*Plasma confinement and transport*" is of specific relevance for the intension of the present lecture.

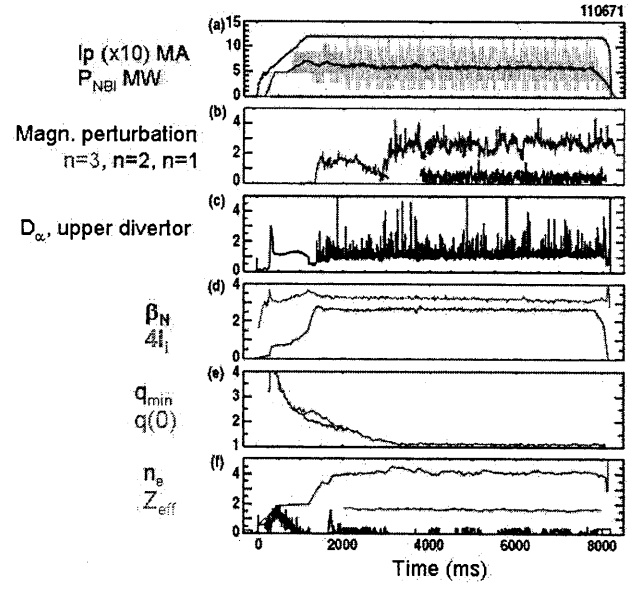

FIGURE 4. High-performance, long-pulse discharge from DIII-D. This discharge, when scaled to ITER, would qualify for Q=10 operation [11].
(Courtesy, T. Luce).

3. THE ELMY H-MODE - BASIC OPERATIONAL REGIME FOR ITER

The basic operational regime for ITER is the ELMy H-mode [8]. This discharge type has been developed to a degree which gives good prospects for Q = 10 operation of ITER. Figure 4 shows such a discharge as developed in DIII-D [11]. The major discharge parameters are constant for about 36 confinement times. The D_α trace indicates the modulation by ELMs. They typically appear during H-mode operation as relaxation processes at the edge, which periodically expel a few percent of the energy and particle content (see chapt. 8.5). Therefore, ELMs allow quasi-steady state operation with controlled impurity levels (see Z_{eff} trace, Fig. 4). The H-mode provides the necessary energy confinement. The good confinement applies, however, to impurities also and indeed the quiescent H-mode, H*, can be terminated by an impurity radiation collapse. In the ELMy H-mode the tasks are split – the low

ence level ensures good energy confinement and the impurity fluxes are lled by edge MHD.

e up to now highest fusion power level of 16.1 MW has been achieved by JET in mode (more the quiescent version) resulting in a Q of 0.65 [2]. 4 MW over 4 s en achieved in quasi-steady state ELMy H-modes.
e H-mode physics will be described in chapt. 8. The main profile characteristics H-mode are the formation of edge pedestals in temperature and density. We will at edge parameters will play a specific role in the development of high core eters. Therefore, the understanding of the edge transport physics and the olation from the present situation to ITER is of specific significance.

4. QUESTIONS TO BE ANSWERED PRIOR TO ITER OPERATION

successfully meet the objectives of ITER depends on many factors and it is y desirable to assess them beforehand by proper extrapolation from the present s and data bases. Major physics questions are:

- Will ITER produce the expected fusion power?
- How sensitive do Q and P_{fus} depend on external parameters e.g. the magnetic field?
- Is the H-mode accessible with the foreseen power of 73 MW? This is – as we have seen – a question of the power threshold.
- What is the pedestal height, specifically that of the temperature?
- What is the density profile shape?
- Will the ITER plasma rotate with internal α-particle heating?
- Will ITER operate in advanced core confinement modes [12]?
- At what n/n_{GW} does the confinement degradation set in (see Fig. 2)
- Will there be sawteeth in the core; what will be their amplitude and period?
- Of course, there are further questions and issues.

he conditions in fusion plasmas are strongly interrelated; the edge pedestal erature enters additively to the core temperature (see chapt. 6). In the H-mode, T_e e edge cannot reach its equilibrium value but the edge gradient is limited by ility boundaries. MHD aspects enter the determination of T_e edge and – because of ile resilience (see chapt. 6) - the core temperature. The projections for $T_{e,ped}$ range veen 2.7 and 5.6 keV which is a large range of uncertainty. As a consequence, Q P_{fus} depend strongly on the rather involved edge physics.
he density profile shape can govern the type of predominant turbulence and the ulence level. But it can also decide on the flow of impurities, whether there is a ng neo-classical inward term or not. In case the pressure is limited, a peaked sity profile can lead to flatter T-gradients and lower core values – again affecting overall performance.
The toroidal rotation of a 2-dim tokamak core plasma can be driven by external mentum input (e.g. by tangential neutral beam injection – however with low torque

in case of ITER) but also spontaneously, driven by the pressure gradient and possibly unbalanced flows in the scrape-off layers. Toroidal flow can improve the overall plasma stability and it can also improve confinement and lead to attractive core parameters. The level of core rotation in ITER is an unresolved issue.

Another issue which is addressed by transport modelling is the robustness of the ITER operational point (Q = 10, P_{fus} = 500 MW) against variation of external parameters like the magnetic field. The ITER performance drops to ~ 70% at a field which is 10% less than the nominal value of 5.3 T [13].

5. PREDICTIONS BY SCALINGS

Figure 3 shows the result of the regression analysis of the energy confinement time on "engineering" parameters like B, I_p, the heating power P, the density n, the isotope mass A_i and geometrical parameters. The resulting scaling relation is:

$$\tau_{Eth}^{ELMy} = 0.0562\, I_p^{0.93}\, B^{0.15}\, P^{-0.69}\, n^{0.41}\, A_i^{0.19}\, R^{1.97}\, \varepsilon^{0.58}\, \kappa^{0.78}\ (s, MA, 10^{19}\ m^{-3}) \qquad (1)$$

The confinement of ITER according to this scaling (IPB 98(y,2)) is 3.7 sec. In this scaling, τ_E is considered as dependable variable; the engineering parameters are considered as independent quantities. Correlations of the independent variables introduced e.g. by operational circumstances are often not visible but affect the result.

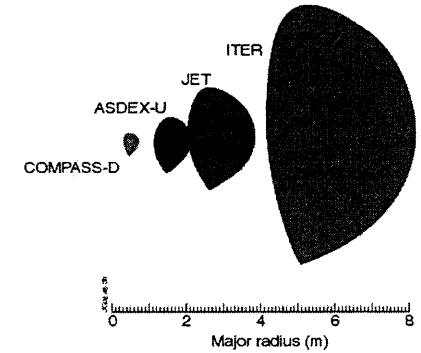

FIGURE 5. Family of devices with nearly identical shape (lower X-point, ellipticity, triangularity) to ITER.

More appropriate and more physically justified is the extrapolation along dimensionless parameters as given by Kadomtsev and Connor and Taylor [14,15]. The relevant ones are ρ^* (normalised ion Larmor radius $\rho_{L,i}/a$), β, and ν^* (collision frequency normalised to a transit frequency (c_S/a)). A recent review on dimensionless scaling is [16]. The basis for the extrapolation to ITER is a set of similarity plasmas which have the geometry and shape parameters of the anticipated ITER plasma, identical profiles and the same T_e/T_i ratio. Relation (1) can be translated into a dimensionless form: $\tau_E B \sim f(\rho^*, \beta, \nu^*)$. The above engineering scaling relation yields in dimensionless form: $\tau_E B \sim \rho^{*-2.7}\, \beta^{-0.9}\, \nu^{*-0.01}$. The ρ^* power is close to -3 which

ms that the overall scaling is gyro-Bohm. This implies that the spatial scale of herent turbulence scales with the Larmor radius $\rho_{L,i}$ (in case of Bohm scaling, ρ^{*-2}; the turbulence spatial scale would go with $\sqrt{a\rho_{L,i}}$). The difference in τ_E of projected from e.g. JET data is a factor ~ 3 between gyro-Bohm and Bohm g.

e β-scaling of $\tau_E B$ is highly unfavourable as fusion power production will occur h β; the scaling with collisionality is weak, which may be surprising having in that ν* represents dissipative processes.

ıereas the IPB 98(y,2) τ_E-scaling obeys the invariance constraints of the basic ıa laws and can be rephrased in dimensionless form, this is not the case for the ıwald density limit and the H-mode power threshold. In case of the density limit, ıt day studies are done at high collisionality; ITER will reach the density limit low collisionality conditions in a possibly different regime.

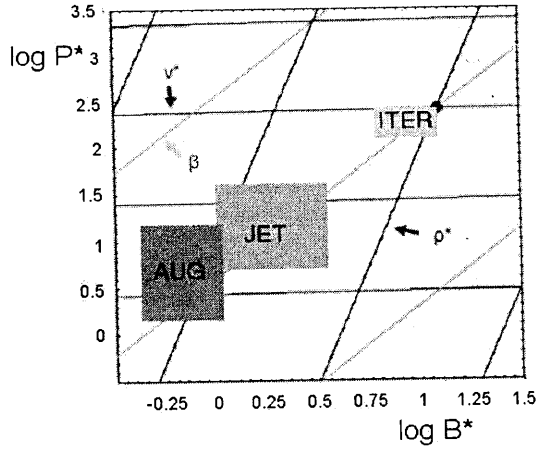

IGURE 6. The operational domains of ASDEX-Upgrade and JET are plotted in the dimensionally ect P*-B* space (see text) along with lines of constant ν*, *6* and ρ*. The ITER target point is also shown [17]. (Courtesy, K. Lackner.)

or practical cases the control parameters have to be transformed into ıensionless engineering variables". A recent summary is given by [16]. onditions for such scaling studies are experiments identical in all geometrical meters. Figure 5 shows plasma cross-sections of such a fleet of devices with ely matched shapes. The dimensionless engineering control parameters are B* ~ ^{1}, P* ~ $P_{heat}\, a^{3/4}$ and n* ~ n $a^{3/4}$/B. For the density, also two other scalings would be ensionally correct. The one is chosen which reproduces the Greenwald scaling est [16]. ρ*, β and ν* can be expressed by B*, P* and n*. Leaving n* constant, the ent day experiments can be plotted in a P*-B* plane whereas the technical ıbilities (B, P) and boundaries for relevant plasma operation determine the limits. ı a diagram is replotted from [16] and shown in Fig. 6. Also the aimed-for ımeters of ITER are given. With the IPB 98(y,2) scaling, which is close to gyro-

Bohm scaling and when n* is selected as constant (representing a constant fraction of n_{GW}), iso-lines of ρ*, ν* and β can be plotted in the P*-B* plane as given in Fig. 6 (for details, please consult the original work [16]).

Present devices cannot operate such that the three dimensionless parameters (ρ*, ν*, β) are fulfilled simultaneously at the ITER targets. They can, however, operate at the β of ITER. The behaviour of ITER in the other parameters can only be deduced via extrapolations along dimensionless scaling experiments. (If the condition n*=const. is given up then operation at the collisionality of ITER is also possible with present devices.) Such scaling studies have been done both within a single device and between devices.

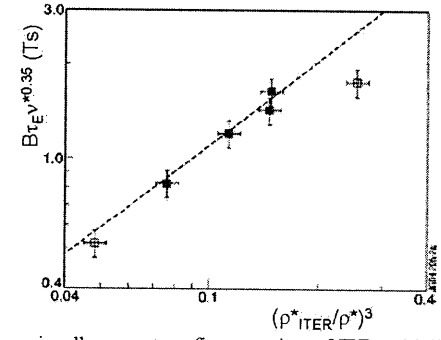

FIGURE 7. The dimensionally correct confinement time of JET multiplied by the empirically obtained ν* scaling is plotted against the ρ* (normalized to ρ^*_{ITER}) displaying the ρ^{*-3} gyro-Bohm scaling [17]. (Courtesy, J. Cordey.)

The scaling of $\tau_E B$ with ρ* from the multi-machine scaling IPB 98(y,2) ($\sim\rho^{*-2.7}$) is close to gyro-Bohm ($\sim \rho^{*-3}$). This ρ* scaling is also born out by devoted scaling studies. Figure 7 shows the results from JET [18]. Plotted is the normalized dimensionless confinement time against the normalised reduced gyro radius. The outcome is a distinct ρ^{*-3} scaling. This is a very valuable result, both from the fundamental nature of turbulent transport and the programmatic goals of fusion.

In a separate study with identical discharges, the β and ν* values of ITER were properly scaled to JET parameters ($I_p \propto B\, a$; $n \propto B^{4/3} a^{-1/3}$; $T \propto B^{2/3} a^{1/3}$; $\rho^* \propto B^{-2/3} a^{-5/6}$) and the gyro-Bohm ρ^{*-3} scaling was applied (see Fig. 7) [17]. For this case the JET parameters (B, n_e, and τ_E) were 3.46 T, 0.96 10^{20} m^{-3} and 0.51 sec. The ITER values were 5.6 T and 2 $10^{20} m^{-3}$). The predicted τ_E was found to vary between 3.74 and 5.6 s and Q from 6.2 to 12.3. The variation of these parameters is due to different transport models employed and a spread in helium concentration [19].

ρ* was varied in the above described experiments via the magnetic field or the temperature. An alternative way to vary ρ_L (= $mv_\perp/eB$) is via the atomic mass A_i, e.g. by comparing hydrogen with deuterium [20] and even tritium plasmas. The observed isotopic dependence of τ_E ($\tau_E \sim A_i^{0.19}$) does, however, not fit into the simple gyro-Bohm scaling. With the gyro-Bohm Ansatz $\tau_E B \sim \rho^{*-3} A_i^{-3/2}$, one obtains for the engineering scaling: $\tau_E \sim A_i^{-0.16}$. The change from e.g. H^+ to D^+ plasmas at identical

ıl settings causes β and ρ* to increase and ν* to decrease. Therefore, also in A_i-
experiments at constant β, ρ* and ν*, a favourable A_i scaling can be expected.
rprising favourable scaling of τ_E with A_i is still an issue to be clarified – to what
it depends on the confinement regime, it is an edge effect (with its own scales
ysics) and why it is not distinct in stellarators.
scaling with the isotopic mass is crucial when one considers the H-mode power
ɔld with a ~ $1/A_i$ scaling [10]. This is favourable for DT operation in ITER but
ɜ a problem for the preceding preparational phase of ITER, which should be in
ɜen or helium to avoid premature activation of the hardware. For hydrogen
ion, the power threshold may be too large (compared to the envisaged power
ɐd of 75 MW); for He the recycling and divertor operational conditions may be
al.

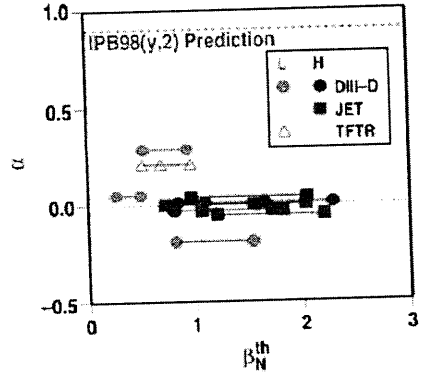

IGURE 8. The exponent of the β-scaling of τ_E ($\tau_E \sim \beta^{\alpha}$) versus normalized beta of devoted scans
ımparison to the expectation from the IPB 98(y,2) confinement scaling [21]. (Courtesy, C. Petty.)

major concern is the β scaling inherent to the IPB 98(y,2) scaling relation ($\tau_E B$ ~
. Again in devoted scans, the β-scaling was investigated in more detail,
ifically matching geometry and profiles of the identity discharges as close as
ible. Figure 8 shows the scaling exponent from various devices, notably from JET
DIII-D in the H-mode, which did not yield a β-dependence at all [21]. These
ngs contradict those of the multi-machine IPB 98(y,2) scaling.
he impact of a β-scaling as inherent to the IPB 98(y,2) scaling and that in case of
-dependence in shown in Fig. 9. Plotted are plasma operation contour (POPCON)
rams (n versus T plane) which allow discussing the approach to the stable fusion
er producing operational point on the background of operational limits or
ational conditions [21]. As reference, iso-lines of constant Q, β_N and P/P_{LH} are
n. Case (a) reflects the IPB 98(y,2) β-scaling and shows that Q eventually
eases along a path from low pressure to high pressure whereas for case (b),
ıout a β-scaling and the assumption of exclusive electrostatic turbulence, the
ease in pressure pays off in a continuous increase in Q.

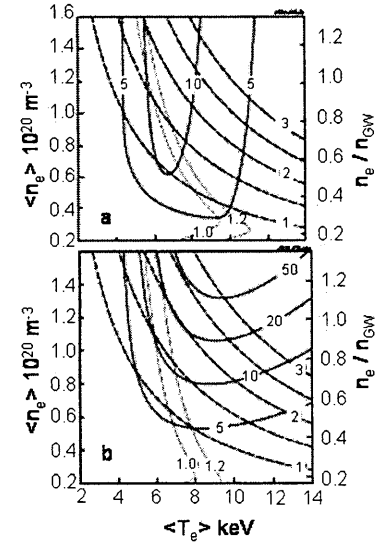

FIGURE 9. ITER operational space in the form of an $\langle n_e \rangle$ (respectively the density normalized to the Greenwald value) versus $\langle T_e \rangle$ POPCON diagram with constant lines of β_N and Q. a) based on the IPB 98(y,2) τ_E scaling ($\tau_E B \sim \beta^{-0.9}$);
b) based on a $\tau_E \sim \beta^0$-scaling) [21]. (Courtesy, C. Petty.)

Let us turn now to the 3rd dimensionless scaling parameter, the normalized collision frequency ν*. The most conspicuous impact of a decreasing collisionality ν* is a peaking of the density profile [22]. The observations (see Fig. 10) agree with the expectations from theory [23]. One has to expect peaked density profiles for ITER. It is difficult to predict what the impact of this feature will be on the core temperature, the prevailing turbulence and the impurity transport and core impurity concentration.

In summary, dimensionless scaling gives an ITER confinement time of 3.3 s which compares well with that of the scaling along engineering parameters (3.7 s). Nevertheless, critical issues remain and cannot be clarified at the moment. The most critical one seems to be the β-scaling of τ_E; the $\tau_E B \sim \rho^{*-3}$-scaling seems to be well established but the isotope scaling does not fit to it. Obviously, it is introduced not as an implicit dependence of ρ* rather by another physics property. The isotope scaling is rather fundamental and is observed in many confinement regimes where different types of small-scale fluctuations prevail (which, of course, should all give rise to gyro-Bohm scaling). The issue of the isotopic scaling is crucial for ITER because the H-mode power threshold depends linearly on ion mass. In case the isotopic effect is introduced by specific edge physics, deviations from gyro-Bohm scaling can be expected from other parameters entering the transport physics.

ıe role of collisionality ν* is well documented and also backed by theoretical iderations. The consequences of peaked density profiles, which have to be cted for ITER, are, however, not clear.

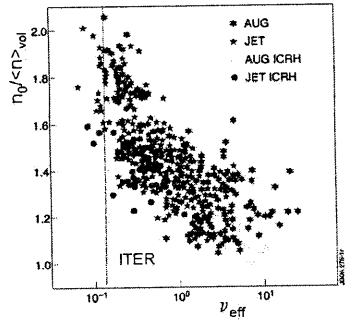

IGURE 10. The density profile peaking factor $n_0/<n>$ versus collisionality. The ν_{eff} value of ITER is indicated [22, 27].

6. MAJOR TRANSPORT CHARACTERISTICS OF TOKAMAK PLASMAS

The discussion on dimensional as well as dimensionless scaling has shown that a er understanding of the inherent turbulent transport in tokamaks is necessary to ntually come to a better prediction of the ITER confinement and related properties. specific interest is, of course, to stabilize the predictions on the accessibility of ıroved confinement regimes for ITER. In this chapter we summarise some of the ıor confinement characteristics of tokamak transport, which seem to be generic and uire theoretical understanding to enhance the predictive capabilities.

The neo-classical transport theory [3] based on particle orbits in toroidal geometry binary collisions is well established. Transport properties parallel to the magnetic d (bootstrap current, neo-classical correction to the electrical conductivity, flow ıping, ion/α-particle slowing down) and the radial electric field, E_r, are generally ll described by this theory. Also the convective part of impurity transport (inward - ward velocities) agrees well with neo-classical expectations. For radial fluxes, the heat transport can be close to neo-classical dissipation at high density or within ernal transport barriers (ITBs). Also the neo-classical particle pinch (Ware-pinch) is observed in the plasma core or at high collisionality. Normally, however, ticle, electron- and ion-heat and momentum transport are anomalous, determined turbulent plasma processes.

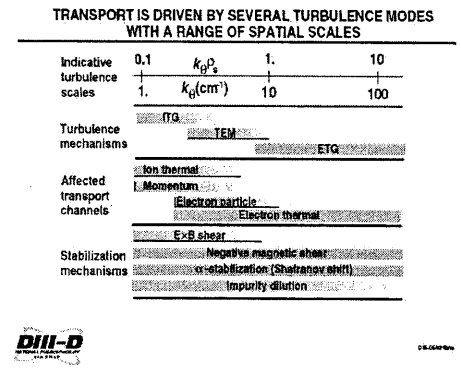

FIGURE 11. Major modes responsible for turbulent transport in toroidal systems with their spatial scales along with the transport channels they potentially affect and the mechanisms which potentially stabilize them [24]. (Courtesy, E. J. Doyle.)

A frequently quoted overview over the most predominant turbulent mechanisms, all different realizations of inherent drift-wave like turbulence, is given in Fig. 11 [24]. With decreasing scales (increasing $k_\theta\rho_S$) they are the ion temperature gradient (ITG) mode, the trapped electron mode (TEM) and the electron temperature gradient (ETG) mode. The diagram also shows which fluxes are driven by these modes and which processes can stabilize them. The most prominent stabilizing mechanism is shear flow stabilization, which is most effective for long-wavelength instabilities (ITG and TEM) (see chapt. 8.2).

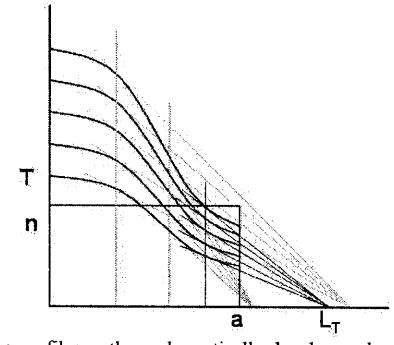

FIGURE 12. Temperature profiles as they schematically develop under profile resilient conditions. The density is flat inside the plasma with radius a. L_c is the gradient length.

Rather early in the search for the major transport characteristics of tokamak plasmas the feature of profile stiffness was discovered [25]. Originally, it was considered as a property of electron transport. With strongly neutral injection heated plasmas, where the ion pressure dominates, it became clear that stiffness also governs the ion temperature profile. The density profile can hardly be described as being stiff.

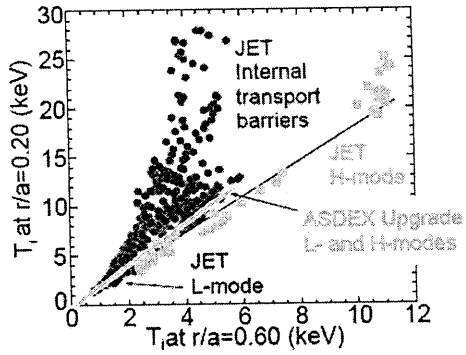

FIGURE 13. The core ion ($T_i(0.2)$) versus the edge ion temperature ($T_i(0.6)$) for L and H-mode charges of JET and ASDEX upgrade (only average relation). In case of JET, the results for profile resilient regimes (L- and H-mode) are compared with relations when an ITB is formed [27].

Profile stiffness addresses the feature that the respective temperature profile shape is not change with the location of the power deposition, when the heating power is reased or the transport changes. Indeed, also in the H-mode, T_e and T_i are found to resilient. The relevant quantity which seems to be fixed is the $-T/\nabla T = L_T$.
The extent of profile resilience and the viability of the concept could be judged by nparison with stellarator profiles, where the property of profile stiffness is not served [26].

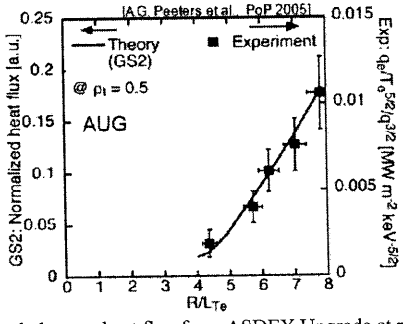

FIGURE 14. Experimental electron heat flux from ASDEX Upgrade at r/a=0.5 versus the reduced e-gradient length in comparison with heat flux calculated on the basis of TEM turbulent modes with the GS2 code [28]. (Courtesy, A. Peeters.)

Figure 12 shows a schematic of a profile development with increasing heating wer, where the gradient lengths are constant. The energy content of such plasmas (at nstant density n_a) is given by

$$W = 4\pi^2 R \int nTrdr = 4\pi^2 R n_a T(a) \int_0^a e^{\int_r^a d\rho / L_T} rdr \propto p(a) \qquad (2)$$

and linearly dependent on the edge pressure p(a). The exponential factor comes from the integration of $-1/T\ dT/dr = 1/L_T$. In case of profile stiffness, the physics of edge pedestals plays a specific role. This topic will be addressed in chapt. 8.

Figure 13 shows the essence of profile stiffness for ion temperature profiles for JET and ASDEX Upgrade both for L- and H- mode plasmas [27]. A strict linear relation between the core and the edge value prevails for the power scans irrespective of the confinement regime.

The physics behind this behaviour are instabilities which respond with a strong increase in turbulent flux as soon as a critical temperature gradient is reached. In toroidal systems, the precise critical condition scales with R/L_T with $T=T_i$ for ITG and $T=T_e$ for TEM modes. Experimental studies clearly reproduce these aspects. Figure 14 shows such a case – now for the electron temperature – resulting from a study done on ASDEX Upgrade [28]. Plotted is the normalized heat flux against R/L_{Te}; the experimental results are compared with theory and both the critical $(R/L_{Te})_{crit}$ and the slope of the relation are reproduced. The slope of the relation shown in Fig. 14 depends critically on the growth rate of the inherent mode.

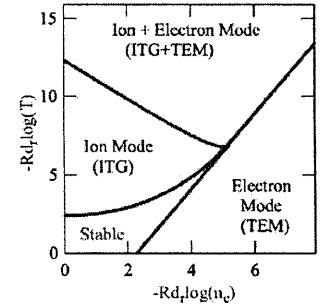

FIGURE 15. Stability R/L_T (with $T_e=T_i$) versus R/L_{ne} diagram for ITG and TEM instabilities [23]. (Courtesy, X. Garbet.)

An important and also very critical topic is the density profile shape [29]. Density profiles with steep gradients give rise to driftwave-like turbulence. But a peaked density profile shape can also stabilize ITG modes because of the expansion and compression work of the interchange process in a situation of negative compressibility. Unlike the heat transport, the source for the particle transports is primarily located at the plasma edge. Density gradients in the source-free region are (generally) caused by turbulent fluxes. On the other hand, the density gradient regulates the stability conditions for the instabilities underlying the turbulence. This gives rise to a highly non-linear situation and attributes a specific role to the density profile. Figure 15 plots another frequently quoted diagram, the existence and co-existence diagram of the major turbulence modes and mechanisms responsible for anomalous transport [23].

Plotted in Fig. 15 is the relative temperature gradient (T_e or T_i, respectively) against the relative density gradient, which are the thermal drives for the instabilities under

nsideration. This plot shows where the different instabilities dominate and indicates ; borders between them. The diagram also shows the critical gradient $\nabla T_{i,crit}$ onset ndition for ITG modes and it demonstrates how ITG turbulence is stabilised by the nsity gradient.

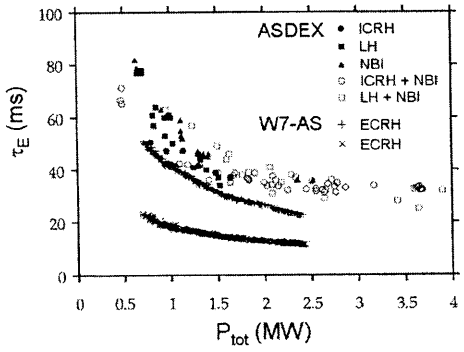

FIGURE 16. L-mode scaling of τ_E with heating power P for different heating methods in ASDEX ld) and with ECRH in W7-AS stellarator. The W7-AS data are scaled by $Vol_{ASDEX}/Vol_{W7\text{-}AS}$ (=5.2) to ow better comparison. Results for two densities are shown: + $n_e = 2\ 10^{19}\ m^{-3}$; × $n_e = 4\ 10^{19}\ m^{-3}$.

7. IMPROVED CONFINEMENT REGIMES

The next topic I want to turn to are improved confinement regimes, the physics hich gives rise to them and their accessibility under ITER conditions.

As soon as toroidal plasmas were auxiliary heated beyond the ohmic level – the rst experiments were done beginning of the 70ties – the catastrophic experience has een made that the energy content did not rise proportionally to the heating power but at all confinement times degraded [30]: that for energy, particles, impurities, and – bserved later - toroidal momentum. The consequence was that the approach to the itical triple product by the increase of the temperature was off-set by the reduction of ıe confinement time. This degradation is fundamental and applies to tokamaks and ellarators, is basically independent of the heating method and is the case for egraded (L-mode) and improved (H-mode) plasmas. This degradation of τ_E with eating power P is shown in the regression (1) and scales like: $\tau_E \sim P^{-0.69}$. Figure 16 ows results from ASDEX (tokamak) and W7-AS (stellarator) with the confinement me scaled by volume.

The H-mode was discovered 25 years ago [31] at the "old" ASDEX. Figure 17 hows two density traces (n_e), one of an L-mode and one of an H-mode discharge aken shortly after the H-mode discovery in 1982. The external parameters of the two ischarges of Fig. 17, which decided on the mode developing during the neutral ajection phase (NBI), was the selected target density of the preceding ohmic phase. he density drop in the L-mode was caused by a reduction of the particle confinement rom the ohmic level; in the H-mode, particle confinement improved leading to a steep ise in n_e after an initial short L-mode period. The importance of the H-mode was

obvious from the beginning on because the energy content increased substantially at constant heating power.

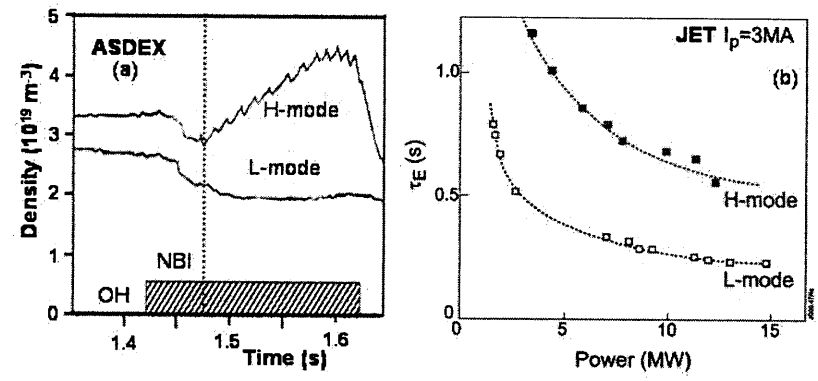

FIGURE 17. Left: (a) line density starting in the ohmic phase into neutral injection for an L-mode and an H-mode discharge in ASDEX (old) [37];
(b) τ_E power scaling in L- and H-modes of JET [2].

Fig. 17 b shows that the energy confinement time is about a factor of 2 above the L-mode level of JET [2] (as it is typical for other machines also and led to the introduction of the improvement factor $H = \tau_E^H/\tau_E^L$). But also in the H-mode, τ_E is observed to degrade with heating power.

The following observations were made in the initial H-mode campaigns:

(1) L- and H-modes differ in confinement time by about a factor of two: two operational branches exist for a given setting; the space in between is not accessible; the H-mode transition can be seen as bifurcation (or phase transition).

(2) All confinement characteristics which degrade in the L-mode - energy, particle, impurity and momentum confinement - improve simultaneously at and after the H-transition.

(3) The H-mode transition requires a minimal heating power P_{LH}: Obviously, a critical condition has to be met which can operationally be achieved by sufficient heating.

(4) There is a dwell time after the heating power has been increased from the ohmic level, before the plasma transits into the H-phase. The dwell time depends on external parameters and is shorter at higher power. It also depends strongly on the magnetic configuration and can be shorter under single- instead of double-null configuration.

(5) When the heating power has been switched off, the plasma remains in the H-phase for a dwell time in the order of the confinement time: After the forward L-H transition, the plasma obviously does not hover at the transition conditions but moves deeper into the H-mode domain; when the external drive is turned off, there is a reserve, which allows the plasma to initially remain in the H-phase. Of significance is that the back transition is not gradual but also occurs in a distinct step – corresponding to the gap between the H- and L-mode branches.

(6) There is also a density threshold; at low density, the critical transition condition not be met. Later it was observed that machine characteristics like radiation and de-locking affects the low-density power threshold [32].
(7) Large sawteeth were found to trigger the H-mode: the critical transition ameter, which can be met by heating beyond the threshold, seems to be a local idition at the plasma edge, which can also be met by a thermal wave from the core sma.
(8) ELMs appeared in the H-mode as a new type of edge localized MHD instability e Fig. 4) [33]; there are operational ways to suppress ELMs. In the quiescent H*-de the intrinsic confinement of the H-mode can be studied. This regime is, however, mally transient because of continuous increase of impurity concentration minated by a disruption or a radiative collapse.

The power threshold was found to be lower for the following cases:
(1) with separatrix instead of limiter operation;
(2) in deuterium instead of hydrogen plasmas; the actual value of P_{LH} depends on isotopic mix. The threshold power for deuterium plasmas has the following ling: $P_{LH} \sim n^{0.73}B^{0.74}S^{0.98}$ ($10^{20}m^{-3}$, MW, T). It is – at otherwise identical conditions a factor of 2 larger in H than D. The isotope scaling is a fundamental problem cause dissipation processes residing on collisions or on medium-scale fluctuations uld not easily explain it. The programmatic issue with the isotopic effect is the estion, whether the heating power of ITER is sufficient to attain the H-mode with drogen. Hydrogen operation is foreseen in the initial period of system and scenario timisation avoiding activation of the device. Alternatively, helium can be used. The wer threshold of He is similar to that of deuterium [34]; He-plasmas have, however, viating recycling and divertor characteristics.
(3) in clean (with boronisation) instead of dirty plasmas;
(4) with gas fuelling from the divertor chamber or the high-field side instead of the w-field side. These aspects entered later into the discussion of the impact of divertor sure on τ_E and P_{LH} [35].
(5) in singe null (SN) plasmas with the ion-grad B-drift to (SN^+) instead of away N^-) from the active X-point; in double-null (DN) plasmas, P_{LH} was found to lie tween the extreme values [36]: Obviously, an unknown mechanism whose impact is rmally expressed as ion-grad-B ($B\times\nabla B$) drift direction in relation to the X-point cation, contributes with a supporting (or prohibiting, respectively) effect, which was llified in ASDEX in the symmetric DN case. At a heating power, sufficient to get e H-mode under DN conditions, the dwell-time prior to the transition is shortened by out a factor of two if operated under SN^+ conditions (see Fig. 101 of Ref. [37]). nder SN^- conditions, the dwell-time could be longer than the NBI pulse.

8. UNDERSTANDING OF THE H-MODE

Many review papers present the status of H-mode research and H-mode derstanding. A recent one [38] is written on the level of a summer school. The ader is invited to consult this and other papers [39, 40, 41]. As this material is easily

available and at an adequate level, the physics of the H-mode will be sketched here without many details.

8.1 Development of an edge transport barrier

At the H-mode transition the turbulence in a small edge layer inside the separatrix disappears with a time scale which can be as short as a few μsec. As this causes a local improvement of confinement, the edge pressure gradient steepens and an edge transport barrier forms [42]. As a consequence, the H-mode transition changes significantly all parameter profiles: Temperature and density profiles adopt pedestals at the edge with close to neo-classical ion and reduced electron heat and particle fluxes. The extent of the transport barrier coincides with the zone of strongly reduced turbulence level. The profiles inside the barrier remain resilient. This fact strengthens the importance of the H-mode according to the arguments given above (see equ. 2) – the energy content scales with the pedestal of the edge pressure.

8.2 Turbulence de-correlation by sheared flows

Rather well established mechanisms capable of explaining the quench of the turbulence within the transport barrier is the interaction of the turbulence velocity field with the background flow. In case this flow is sheared – has a gradient – the turbulence size scales are reduced perpendicular to the mean flow [43]. Within a random-walk view, the reduction of the radial transport can be seen from $D \sim \Delta x^2/\Delta t \sim \gamma/k_\perp^2$, with γ being the rise time and $k_\perp^{-1}$ the radial extent of turbulent eddies. This mechanism requires that the shearing rate, the flow gradient, $\omega_{E\times B} > \gamma_{lin}$, γ_{lin} being the linear rise time of the turbulence. It is experimentally verified that this relation is not obeyed in the L-mode and that the shearing rate compares within the error bars with the rise time at the transition [44].

8.3 Edge electric field development

The plasma equilibrium gives rise to a deep radial electric field well [45] within the transport barrier to confine the ions [46]. This development causes a strong rotation of the plasma within the gradient region. The steady-state radial electric field has in its simplest formulation two constituents - the diamagnetic contribution and the $v \times B$ components:

$$E_r = 1/Zen_e\nabla p_i - v_\theta B_\phi + v_\phi B_\theta \qquad (3)$$

∇p_i is determined by the power balance involving heat and particle sources and sinks and – prior to the transition - L-mode transport. There is overall agreement that this component plays indeed a significant role after the H-transition: The ∇p_i– term develops within a confinement time, deepens the E_r-well at the edge and stabilises the H-mode turbulence decorrelation condition [47,48].

Right at the H-mode transition, the situation is different. The involved time scales are much shorter than those of transport. Polarisation experiments have shown that E_r is the lead term and ∇p_i is found to lag behind [48,49]. The conclusion from this chain

of action is that E_r (or E_r', respectively) is obviously the cause of the transition, which consecutively leads to the increase in ∇p_i.

The observations reported above show that the $\mathbf{v} \times \mathbf{B}$ components contributes to the radial electric field and may even be the decisive transition trigger [50]. The $\mathbf{v} \times \mathbf{B}$ term introduces poloidal and toroidal momentum balances into the transition physics including neo-classical equilibrium characteristics and anomalous transport features.

The inclusion of v_θ into the transition physics opens a rich field of potential transition mechanisms [39]. v_θ is given by the poloidal momentum balance of torques from radial electric currents and poloidal damping. The steady-state momentum balance comprises of the Lorentz force term, the poloidal damping term, the friction term with the ambient neutrals and the turbulent Reynolds stress term. This term is of special interest because it allows the transfer of energy from the turbulent field into a steady flow – a mechanism which plays an important role in conventional Navier-Stokes systems – the atmosphere of the Earth or of planets, the ocean and in laboratory turbulence set-ups.

8.4 A possible paradigm of the H-mode transition

The verification of the H-mode transition on the basis of self-induced flows, so called Zonal Flows [51], which may be of stationary or oscillating nature and which annihilate their initially driving mechanism, requires rather detailed knowledge of spatial and temporal structures of the edge turbulence. The following picture emerges from detailed studies at the H-1 heliac [52]. Drift wave based turbulence is caused by the pressure gradient of the L-phase. Energy cascades from the injection-k to lower k-values by three-wave interaction. In other words, the modes "condense" via a non-local spectral transfer process, connecting different size scales, into coherent structures and the spectral energy accumulates at the largest possible scale: Energy couples from the large k-domains, energized by the pressure gradient, to the m = 0 mode. Oscillating zonal flows appear, with a structure corresponding to the largest possible system size, the poloidal circumference. The oscillating zonal flows, the GAMs [51], represent a seed for the H-transition.

8.5 ELMs

The edge pressure gradient is normally limited in the H-mode by the stability condition for the ELMs, the edge localised modes [53]. An ELM releases a pulse of energy and particles from the plasma edge with $\Delta W/W \sim \Delta N/N \sim$ 5-10%. (N represents the particle content of the plasma.) The ELMs represent, however, a hazard for the divertor target plates of ITER because the power fluxes can be excessively large (20 MW/m^2 and above).

As these relaxations appear with certain regularity, the average effect corresponds to a degradation of the energy confinement. This reduction is not caused by enhanced fine-scale turbulence but by global MHD. Between the ELMs, the confinement can be at the level of the neo-classical ion heat transport. The effective limitation of confinement and the definition of the average profile by a repetitive MHD process is one of the difficulties to understand and project the radial extent and the height of the

edge pedestal and along with it its impact on confinement. In addition, the short gradient lengths within the transport barrier can give rise to the breakdown of standard transport ordering.

The ELMs are analysed as edge peeling-ballooning modes which are triggered by the local current density and pressure gradients [54]. It is the bootstrap current at the edge which contributes with the peeling mode character of the instability. These drives apply to (conventional) stellarators too, which also show ELMs under typical H-mode conditions [55].

8.6 Further development of H-mode operation

Apart from the understanding of the H-mode transition, which is not yet understood to an extent that modelling of transitions would be possible, the programmatic development has the goal to improve the H-mode quality further and to find means to suppress ELMs without causing impurity accumulation problems. Improved H-modes are indeed observed with H-factors as large as ~ 1.5 [56,57]. Often, the further improvement goes at the expense of higher power thresholds.

Several ways are explored to avoid ELMs. One way is to destabilise the plasma edge in a controlled form and trigger ELMs frequently by e.g. small pellets [58], which increase the edge pressure via the density and cause a small and technically manageable ELM or by ergodizing the plasma edge via a set or resonant perturbation coils [59]. In this case, the parallel transport is expected to keep the edge current and pressure gradients at a level below the critical one. Both methods have demonstrated their effectiveness. It is foreseen, to install perturbation coils into ITER; for larger m components, they have to be placed close to the plasma and are a considerable technical burden.

Quiescent H-modes are possible without ELMs and without major impurity problems [57, 60, 61]. In such cases, quasi-coherent modes are observed, which reside close to the plasma edge and which could give rise to effective impurity diffusion. It could be that such modes, when located within the steep gradient region, on one hand limit the pressure gradient and, on the other, expel impurities. The optimisation of such H-mode variants and the extension of their operational range would be a rewarding goal. There is specific hope for success because such modes appear in helical systems also with the same beneficial characteristics [62] – no ELMs and L-mode level impurity confinement. The fact that such operational modes and transport mechanisms appear in stellarators also indicate that H-mode variants without ELMs and impurity confinement at the L-mode level – due to an MHD edge instability – are rather generic to torodial confinement. It might be worthwhile to specifically generate such plasmas.

ACKNOWLEDGEMENT

I want to thank all those who have allowed me to use already published diagrams.

REFERENCES

[1] K. Lackner, 1958 - 2008: *50 Jahre Fusionsforschung für den Frieden*, in: *50 Jahre Plasmaphysik und Fusionsforschung in Innsbruck* (ed. A. Kendl), Innsbruck University Press, 2008.
[2] M. Keilhacker et al., *Nuclear Fusion*, **41**, 1925 (2001).
[3] J. Wesson, *Tokamaks*, 3rd edition, Oxford Science Publishing, 2004.
[4] E.J. Doyle et al, *ITER Physics Base*, Nuclear Fusion **47**, S18 (2007).
[5] M. Greenwald, *Plasma Phys. Control. Fusion*, **44**, R27 (2002).
[6] F. Troyon, *Plasma Phys. Control. Fusion*, **30**, 1597 (1988).
[7] G. Saibene, et al., *Plasma Phys. Control. Fusion*, **44, 1769** (2002).
[8] ITER Physics Basis 1999 *Nuclear Fusion*, **39**, 2175 (1999).
[9] J.A. Snipes et al., *Plasma Phys. Control. Fusion*, **42**, A299 (2000).
[10] J.A. Snipes et al., *Nucl. Fusion* **36**, 1217 (1996).
[11] T. Luce et al., *Nucl. Fusion* **45**, 86 (2005).
[12] R. C. Wolf, *Plasma Phys. Control. Fusion*, **45,** R1 (2003).
[13] R. V. Budny et al., *Nucl. Fusion*, **48**, 1 (2008).
[14] B. B. Kadomtsev, *Tokamak Plasma: A Complex Physical System*, Institute of Physics Publishing, Bristol, 1992.
[15] J.W. Connor and J.B. Taylor, *Nucl. Fusion*, **17**, 1047 (1977).
[16] T.C. Luce, C.C. Petty and J.G. Cordey, *Plasma Phys. Control. Fusion*, **50,** 1 (2008).
[17] K. Lackner, *Fusion Science & Technology*, **54**, 341508 (2008).
[18] G. Cordey et al., Proc. 31st. EPS Conf. on Plasma Physics (London, 2004), ECA Vol. 28G, O-1.05 (2004).
[19] V. Mukhovatov et al., *Nucl. Fusion*, **43**, 942 (2003)
[20] M. Bessenrodt-Weberpals, et al., *Nucl. Fusion*, **33**, 1206 (1993).
[21] C.C. Petty et al., *Phys.Plasmas*, **11**, 2514 (2004).
[22] C. Agnoni et al., *Phys.Plasmas*, **10**, 3225 (2003).
[23] X. Garbet, et al., *Plasma Phys. Control. Fusion*, **46,** B557 (2004).
[24] E.J. Doyle et al., *Plasma Physics and Contr. Nucl. Fusion Research 2008* (Proc. 18th Int. Conf. Sorrento, 2000), paper EX6/2.
[25] B. Coppy, *Comments Plasma Phys. Controlled Fusion*, **5**, 261 (1980).
[26] F. Wagner et al., *Phys. Rev. Lett.*, **56**, 2187 (1986).
[27] X. Litaudon, *Plasma Phys. Control. Fusion*, **48, A1** (2006).
[28] A.G. Peeters et al., *Phys.Plasmas* **12**, 022505 (2005).
[29] F. Wagner and U. Stroth, *Plasma Phys. Control. Fusion* **35**, 1321 (1993).
[30] R. Goldston, *Plasma Phys. Control. Fusion*, **26**, 87 (1984).
[31] F. Wagner et al., *Phys. Rev. Lett.*, **49**, 1408 (1982).
[32] T.N. Carlstrom and R.J. Groebner *Phys. Plasmas*, **3**, 1867 (1996)
[33] M. Keilhacker et al., Plasma Phys. Contr. Fusion 26, 49 (1984)
[34] F. Ryter et al., *Plasma Physics and Contr. Nucl. Fusion Research 2008* (Proc. 22th Int. Conf. Geneva, 2008), to be published.
[35] F. Wagner, et al., *Plasma Physics and Contr. Nucl. Fusion Research 1991* (Proc. 13th Int. Conf. Washington DC, 1990), Vol. 1, IAEA, Vienna (1991) 277.
[36] F. Wagner et al., *Nucl. Fusion* **25**, 1490 (1985).
[37] ASDEX team, *Nucl. Fusion*, **29**, 1959 (1989).
[38] F. Wagner, *Turbulent Transport in Fusion Plasmas*, 1st ITER International Summer School, ed. S. Benkadda, American Institute of Physics, Melville, 2008, p. 143.
[39] J.W. Connor and H.R. Wilson, *Plasma Phys. Contr. Fusion* **42**, R1 (2000).
[40] F. Wagner, *Plasma Phys. Control. Fusion*, **49**, B1 (2007).
[41] P.W. Terry, *Rev. Mod. Phys.*, **72**, 109 (2000).
J. Hugill, *Plasma Phys. Control. Fusion*, **42**, R75 (2000).
K.H. Burrell, *Phys. Plasmas* **6**, 4418 (1999).

K. Itoh and S.-I. Itoh, *Plasma Phys. Contr. Fusion*, **38**, 1 (1996).
[42] F. Wagner et al., *Phys. Review Letters* **53**, 1453 (1984).
[43] H. Biglary, P.H. Diamond, and P. W. Terry, *Phys. Fluids* **B 4**, 1385 (1990).
[44] M. Jakubowski, R.J. Fonck and G.R. McKee, *Phys. Rev. Lett.* **89** 265003-1 (2002).
[45] K. Itoh and S-I Itoh, *Plasma Phys. Contr. Fusion*, **38**, 1 (1996).
[46] R. J. Groebner, K. H. Burrell and R. P. Seraydarian, *Phys. Rev. Lett.* **64,** 3015 (1990).
[47] F. Wagner et al., In: *Plasma Physics and Controlled Nuclear Fusion Research* 1990, **Vol. 1**, 277-290, Nuclear Fusion Supplement, 1991, IAEA-CN-53-A-IV-2, (1991).
[48] K.H. Burrell, *Phys. Plasmas* **6**, 4418 (1999).
[49] S. Jachmich et al., *Plasma Phys. Control. Fusion*, **40**, 1105 (1998).
[50] R.A. Moyer et al., *Phys. Plasmas* **2**, 2397 (1995).
[51] P. H. Diamond, S-I Itoh, K. Itoh and T.S. Hahm, *Plasma Phys. Control. Fusion*, **47,** R35 (2005).
[52] M.G. Shats et al., *Phys. Rev.* E, **71,** 046409 (2005).
[53] H. Zohm, *Plasma Phys. Control. Fusion*, **38**, 105 (1996).
[54] J. W. Connor, *Plasma Phys. Control. Fusion*, **40**, 191 (1998).
[55] F. Wagner, *Plasma Phys. Control. Fusion*, **48**, A217 (2006).
[56] W. Suttrop et al., *Plasma Phys. Control. Fusion*, **46**, A151 (2004).
[57] K. H. Burrell et al., *Plasma Phys. Control. Fusion*, **44**, A253 (2002).
[58] P. T. Lang et al., *Nucl. Fusion*, **48,** 095007 (2008).
[59] T. E. Evans et al,. *Phys. Rev. Lett.* **92**, 235003 (2004).
[60] I. Hutchinson et al., *Nucl. Fusion*, **41,** 1391 (2001).
[61] K. McCormick et al., *Phys. Rev. Lett.*, **89,** 015001 (2001).
[62] E. Belonohy et al. *34th EPS Conf. on Plasma Physics (Warsaw, Poland)* 2007.